A dynamic global-coefficient subgrid-scale model for large-eddy simulation of turbulent scalar transport in complex geometries

By D. You AND P. Moin

1. Motivation and objectives

The "local-equilibrium" hypothesis that assumes a local balance between the viscous dissipation and the subgrid-scale dissipation at the same physical location in turbulent flow has been commonly used for turbulence modeling. For example, based on the local equilibrium hypothesis, Germano *et al.* (1991) and Moin *et al.* (1991) developed dynamic procedures for determining the model coefficients of the Smagorinsky-model-based subgrid-scale eddy viscosity as a function of space and time. The local equilibrium assumption results in both favorable and unfavorable consequences to large-eddy simulation. The dynamic modeling procedure allows vanishing eddy viscosity by the model coefficient vanishing in regions where the flow is laminar or the eddy viscosity should be zero. However, the dynamic model coefficient can cause numerical instability since its value often becomes negative and/or highly fluctuates in space and time. The unfavorable feature of the dynamic model coefficient is closely related to the fact that the chance of local equilibrium between the subgrid-scale dissipation and the viscous dissipation is low as observed by da Silva & Metais (2002) and Borue & Orszag (1998). Therefore, the numerical instability has been remedied by additional numerical procedures such as an averaging of the model coefficient over statistically homogeneous directions or an *ad hoc* clipping procedure (*e.g.,* Meneveau *et al.* 1996). However, the numerical stabilization procedure becomes complicated when the dynamic model is applied to a complex flow configuration in which there are no homogeneous directions.

The shortcoming of the dynamic Smagorinsky models based on the local-equilibrium hypothesis was overcome by Park *et al.* (2006). They proposed a dynamic procedure for determining the model coefficient of an eddy-viscosity model developed by Vreman (2004) utilizing a "global equilibrium" hypothesis that assumes a global balance between the subgrid-scale dissipation and the viscous dissipation. However, the dynamic procedure of Park *et al.* (2006) requires two-level test filters of which utilization is difficult and impractical, especially with unstructured grid topology where defining the second-level test filter is not straightforward.

More recently, an improved dynamic procedure for a closure of Vreman's model (2004) has been proposed by You & Moin (2007). The model by You & Moin (2007) also assumes global equilibrium between the subgrid-scale dissipation and the viscous dissipation, and requires only a single-level test filter, which improves the applicability of the model for complex flow configurations. In the global-equilibrium approaches (You & Moin 2007; Park *et al.* 2006), the model coefficient is determined to be globally uniform in space but to vary in time, and does not require any *ad hoc* numerical stabilization or clipping operations. Even with a non-zero constant model coefficient, the global-coefficient models still guarantee zero eddy viscosity in the laminar and fully resolved flow regions by the

inherent advantage of Vreman's eddy-viscosity model (2004) in which vanishing subgrid-scale dissipation for various laminar shear flows is theoretically guaranteed.

The local-equilibrium hypothesis has also been employed for a closure of the subgrid-scale scalar flux (*e.g.,* Moin *et al.* 1991). However, the chance of local balance between the subgrid-scale scalar diffusion and the molecular diffusion is also found to be small, especially at high Reynolds and Schmidt numbers as reported by da Silva & Pereira (2005) in their direct numerical simulations of homogeneous isotropic turbulence. The local imbalance also causes a numerical instability and requires additional numerical procedures such as an averaging of the model coefficient over statistically homogeneous directions or an *ad hoc* clipping procedure (Moin *et al.* 1991).

In this study the global-equilibrium-based modeling approach of You & Moin (2007), which has been successfully utilized for large-eddy simulation of incompressible turbulent flow, is generalized for large-eddy simulation of turbulent flow with scalar transport, especially in complex configurations. The present dynamic procedure assumes "global equilibrium" between the subgrid-scale scalar diffusion and the molecular diffusion. Similarly to the dynamic procedure for determining eddy viscosity (You & Moin 2007), the present model necessitates only a single-level test filter and does not require any numerical stabilization procedures. Therefore the proposed model is suitable for large-eddy simulation of turbulent flow with scalar transport in complex configurations.

A generalization of the dynamic global-coefficient model by You & Moin (2007) to turbulent scalar transport is introduced in Section 2. In Section 3, the predictive capability of the present model is evaluated by considering turbulent channel flow at two different Reynolds and Prandtl (or Schmidt) numbers. A brief summary is presented in Section 4.

2. Global-coefficient subgrid-scale model for turbulent scalar transport

The incompressible continuity, momentum, and scalar transport equations are considered as follows:

$$\frac{\partial u_i}{\partial x_i} = 0, \tag{2.1}$$

$$\frac{\partial u_i}{\partial t} + \frac{\partial u_i u_j}{\partial x_j} = -\frac{\partial p}{\partial x_i} + \nu \frac{\partial^2 u_i}{\partial x_j \partial x_j}, \tag{2.2}$$

$$\frac{\partial \theta}{\partial t} + \frac{\partial \theta u_j}{\partial x_j} = \alpha \frac{\partial^2 \theta}{\partial x_j \partial x_j}, \tag{2.3}$$

where ν and α ($= 1/PrRe$ or $1/ScRe$) are the molecular viscosity and diffusivity, respectively.

By applying a "grid" filter $\overline{()}$ to (2.1)–(2.3), one obtains the following filtered governing equations of motions:

$$\frac{\partial \overline{u}_i}{\partial x_i} = 0, \tag{2.4}$$

$$\frac{\partial \overline{u}_i}{\partial t} + \frac{\partial \overline{u}_i \overline{u}_j}{\partial x_j} = -\frac{\partial \overline{p}}{\partial x_i} + \nu \frac{\partial^2 \overline{u}_i}{\partial x_j \partial x_j} - \frac{\partial \tau_{ij}}{\partial x_j}, \tag{2.5}$$

$$\frac{\partial \bar{\theta}}{\partial t} + \frac{\partial \bar{\theta} \bar{u}_j}{\partial x_j} = \alpha \frac{\partial^2 \bar{\theta}}{\partial x_j \partial x_j} - \frac{\partial q_j}{\partial x_j}, \tag{2.6}$$

where τ_{ij} and q_j are the subgrid-scale stress tensor and scalar flux, respectively. The

subgrid-scale stress tensor τ_{ij} is modeled by an eddy-viscosity model:

$$\tau_{ij} - \frac{1}{3}\delta_{ij}\tau_{ij} = -2\nu_T^g \overline{S}_{ij}, \tag{2.7}$$

where ν_T^g is the eddy viscosity. In the present study an eddy-viscosity model by Vreman (2004) is considered for determining ν_T^g:

$$\nu_T^g = C_v \Pi^g, \tag{2.8}$$

where

$$\begin{aligned}
\Pi^g &= \sqrt{\frac{B_\beta^g}{\overline{\alpha}_{kl}\overline{\alpha}_{kl}}},\\
B_\beta^g &= \beta_{11}^g\beta_{22}^g - \beta_{12}^g\beta_{12}^g + \beta_{11}^g\beta_{33}^g - \beta_{13}^g\beta_{13}^g + \beta_{22}^g\beta_{33}^g - \beta_{23}^g\beta_{23}^g,\\
\beta_{ij}^g &= \sum_{m=1}^{3} \overline{\Delta}_m^2 \overline{\alpha}_{mi}\overline{\alpha}_{mj},\\
\overline{\alpha}_{ij} &= \frac{\partial \overline{u}_j}{\partial x_i}.
\end{aligned} \tag{2.9}$$

$\overline{\Delta}_m$ is the grid-filter width in the m-direction, $()^g$ denotes a grid-filter-level quantity, and C_v is the model coefficient. A novel feature of the model that makes it superior to the Smagorinsky model with a constant coefficient, is that the kernel Π^g becomes zero for canonical cases where the eddy viscosity should be zero. More details of the derivation of the model and its characteristics can be found in Vreman (2004).

You & Moin (2007) proposed a dynamic procedure using a single-level test filter to determine the model coefficient C_v based on a transport equation for L_{ii} $(= T_{ii} - \widehat{\tau}_{ii})$

$$\begin{aligned}
&\frac{\partial L_{ii}}{\partial t} =\\
&\quad \frac{\partial}{\partial x_j}\left\{ -(\widehat{\overline{u}_i\overline{u}_i\overline{u}_j} - \widehat{\overline{u}}_i\widehat{\overline{u}}_i\widehat{\overline{u}}_j) - 2(\widehat{\overline{u}_j\overline{p}} - \widehat{\overline{u}}_j\widehat{\overline{p}}) + \nu\left(\frac{\partial\widehat{\overline{u}_i\overline{u}_i}}{\partial x_j} - \frac{\partial\widehat{\overline{u}}_i\widehat{\overline{u}}_i}{\partial x_j}\right) - 2(\widehat{\tau_{ij}\overline{u}_i} - T_{ij}\widehat{\overline{u}}_i)\right\}\\
&\quad -2\nu\left(\frac{\partial\widehat{\overline{u}_i}}{\partial x_j}\frac{\partial\overline{u}_i}{\partial x_j} - \frac{\partial\widehat{\overline{u}}_i}{\partial x_j}\frac{\partial\widehat{\overline{u}}_i}{\partial x_j}\right) + 2(\widehat{\tau_{ij}\overline{S}_{ij}} - T_{ij}\widehat{\overline{S}}_{ij}).
\end{aligned} \tag{2.10}$$

Taking the volume average of (2.10) assuming "global equilibrium" finally results in

$$C_v = -\frac{\nu}{2}\cdot\frac{\left\langle \widehat{\overline{\alpha}_{ij}\overline{\alpha}_{ij}} - \widehat{\overline{\alpha}}_{ij}\widehat{\overline{\alpha}}_{ij}\right\rangle}{\left\langle \Pi^g\widehat{\overline{S}_{ij}\overline{S}_{ij}} - \Pi^t\widehat{\overline{S}}_{ij}\widehat{\overline{S}}_{ij}\right\rangle}, \tag{2.11}$$

where Π^g is defined in (2.9) and

$$\begin{aligned}
T_{ij} - \frac{1}{3}T_{kk}\delta_{ij} &= -2C_v\Pi^t\widehat{\overline{S}}_{ij},\\
\Pi^t &= \sqrt{\frac{B_\beta^t}{\widehat{\overline{\alpha}}_{kl}\widehat{\overline{\alpha}}_{kl}}},\\
B_\beta^t &= \beta_{11}^t\beta_{22}^t - \beta_{12}^t\beta_{12}^t + \beta_{11}^t\beta_{33}^t - \beta_{13}^t\beta_{13}^t + \beta_{22}^t\beta_{33}^t - \beta_{23}^t\beta_{23}^t,
\end{aligned}$$

$$\beta_{ij}^t = \sum_{m=1}^{3} \widehat{\overline{\Delta}}_m^2 \widehat{\overline{\alpha}}_{mi} \widehat{\overline{\alpha}}_{mj},$$
$$\widehat{\overline{\alpha}}_{ij} = \frac{\partial \widehat{\overline{u}}_j}{\partial x_i}. \tag{2.12}$$

$\widehat{\overline{\Delta}}_m$ is the test-filter width in the m-direction and $()^t$ denotes a test-filter-level quantity.

The present model coefficient is dynamically determined from the instantaneous flow field and computational resolution by utilizing only a single-level test filter. It was found that the temporal variation of the model coefficient is mild and the mean value of the coefficient often quite differs from the fixed value of 0.07 proposed by Vreman (2004) for channel flow and mixing layer simulations (You & Moin 2007).

Besides the advantage of utilizing only a single-level test filter, which improves the applicability of the model for complex flow configurations, the present volume-averaging process in (2.11) obviates a possibility of obtaining different model coefficients when two different computational domains that contain the same turbulent flow field but different laminar shear flow regions are employed. This is because both the viscous dissipation ($\nu(\widehat{\overline{\alpha}_{ij}\overline{\alpha}_{ij}} - \widehat{\overline{\alpha}}_{ij}\widehat{\overline{\alpha}}_{ij})$) and the subgrid-scale dissipation ($\Pi^g \widehat{\bar{S}_{ij}\bar{S}_{ij}} - \Pi^t \widehat{\overline{S}}_{ij}\widehat{\overline{S}}_{ij}$) in (2.11) vanish in the laminar flow region. Therefore, in the present method, the regions where both the subgrid-scale dissipation and the viscous dissipation vanish are naturally excluded from the averaging process in (2.11).

The dynamic modeling procedure based on the global-equilibrium hypothesis is generalized to model the subgrid-scale scalar flux. A transport equation for the scalar variance in the grid-filter level is derived as follows:

$$\frac{\partial}{\partial t}(\overline{\theta^2} - \bar{\theta}^2) = \frac{\partial}{\partial x_j}\left(-(\overline{\theta^2 u_j} - \bar{\theta}^2 \bar{u}_j) + 2\alpha(\theta \overline{\frac{\partial \theta}{\partial x_j}} - \bar{\theta}\frac{\partial \bar{\theta}}{\partial x_j}) + 2\bar{\theta} q_j \right)$$
$$- 2\alpha\left(\overline{\frac{\partial \theta}{\partial x_j}\frac{\partial \theta}{\partial x_j}} - \frac{\partial \bar{\theta}}{\partial x_j}\frac{\partial \bar{\theta}}{\partial x_j} \right) - 2 q_j \frac{\partial \bar{\theta}}{\partial x_j}. \tag{2.13}$$

In a similar way, a transport equation for the scalar variance in the test-filter level can be derived as:

$$\frac{\partial}{\partial t}(\widehat{\overline{\theta^2}} - \widehat{\bar{\theta}}^2) = \frac{\partial}{\partial x_j}\left(-(\widehat{\overline{\theta^2 u_j}} - \widehat{\bar{\theta}}^2 \widehat{\bar{u}}_j) + 2\alpha(\theta \widehat{\overline{\frac{\partial \theta}{\partial x_j}}} - \widehat{\bar{\theta}}\frac{\partial \widehat{\bar{\theta}}}{\partial x_j}) + 2\widehat{\bar{\theta}} Q_j \right)$$
$$- 2\alpha\left(\widehat{\overline{\frac{\partial \theta}{\partial x_j}\frac{\partial \theta}{\partial x_j}}} - \frac{\partial \widehat{\bar{\theta}}}{\partial x_j}\frac{\partial \widehat{\bar{\theta}}}{\partial x_j} \right) - 2 Q_j \frac{\partial \widehat{\bar{\theta}}}{\partial x_j}. \tag{2.14}$$

Extracting test-filtered (2.13) from (2.14) finally results in a transport equation for $\widehat{\overline{\theta}^2} - \widehat{\bar{\theta}}^2$:

$$\underbrace{\frac{\partial}{\partial t}(\widehat{\overline{\theta}^2} - \widehat{\bar{\theta}}^2)}_{T_\theta} = \underbrace{\frac{\partial}{\partial x_j}\left(-(\widehat{\overline{\theta}^2 \bar{u}_j} - \widehat{\bar{\theta}}^2 \widehat{\bar{u}}_j) + 2\alpha(\widehat{\overline{\theta}\frac{\partial \bar{\theta}}{\partial x_j}} - \widehat{\bar{\theta}}\frac{\partial \widehat{\bar{\theta}}}{\partial x_j}) + 2(\widehat{\bar{\theta} Q_j} - \widehat{\bar{\theta} q_j}) \right)}_{\Gamma_\theta}$$
$$\underbrace{-2\alpha\left(\frac{\partial \widehat{\bar{\theta}}}{\partial x_j}\frac{\partial \overline{\theta}}{\partial x_j} - \frac{\partial \widehat{\bar{\theta}}}{\partial x_j}\frac{\partial \widehat{\bar{\theta}}}{\partial x_j} \right)}_{\epsilon_\alpha} \underbrace{-2\left(Q_j \frac{\partial \widehat{\bar{\theta}}}{\partial x_j} - q_j \widehat{\frac{\partial \bar{\theta}}{\partial x_j}} \right)}_{\epsilon_{SGS}}, \tag{2.15}$$

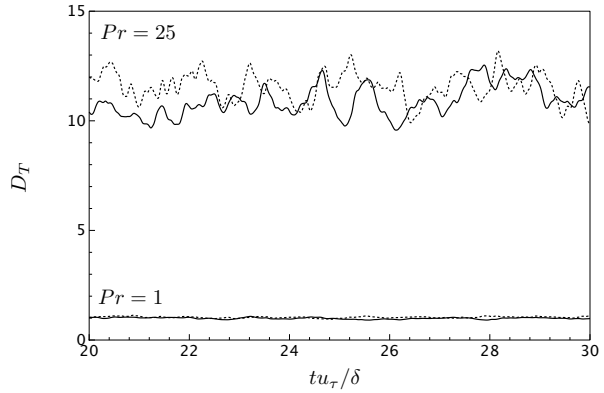

FIGURE 1. Temporal evolution of D_T predicted by the present dynamic procedure for turbulent channel flow at $Re_\tau = 180$ and $Pr = 1$ and 25. ——— , fine mesh LES (LES180F); ····· , coarse mesh LES (LES180C).

where Γ_θ is the redistribution term and ϵ_α and ϵ_{SGS} are the molecular and the subgrid-scale diffusion terms, respectively.

Taking the volume average $\langle\rangle$ of the terms in (2.15) over the entire computational domain assuming that the volume averages of the redistribution term and the time variation term T_θ are negligible, yields

$$D_T = \frac{\left\langle \nu_T^t \frac{\partial\widehat{\overline{\theta}}}{\partial x_j}\frac{\partial\widehat{\overline{\theta}}}{\partial x_j} - \nu_T^g \widehat{\frac{\partial\overline{\theta}}{\partial x_j}\frac{\partial\overline{\theta}}{\partial x_j}} \right\rangle}{\alpha\left\langle \widehat{\frac{\partial\overline{\theta}}{\partial x_j}\frac{\partial\overline{\theta}}{\partial x_j}} - \frac{\partial\widehat{\overline{\theta}}}{\partial x_j}\frac{\partial\widehat{\overline{\theta}}}{\partial x_j} \right\rangle}, \tag{2.16}$$

where

$$q_j = \overline{u_j\theta} - \overline{u_j}\,\overline{\theta} = -\frac{\nu_T^g}{D_T}\frac{\partial\bar{\theta}}{\partial x_j},$$
$$Q_j = \widehat{\overline{u_j\theta}} - \widehat{\overline{u_j}}\,\widehat{\overline{\theta}} = -\frac{\nu_T^t}{D_T}\frac{\partial\widehat{\overline{\theta}}}{\partial x_j}. \tag{2.17}$$

ν_T^g is defined in (2.8) and $\nu_T^t = C_v\Pi^t$.

Similarly to the modeling approach for determining eddy viscosity, the present dynamic procedure for determining turbulent diffusivity requires only a single-level test filter and therefore is easy to utilize for large-eddy simulation in complex flow configurations. The present volume-averaging process also obviates the possibility of obtaining different turbulent diffusivity when two different computational domains that contain the same turbulent flow and scalar fields but different laminar shear flow regions are employed. This is because both the molecular diffusion ($\alpha\widehat{\frac{\partial\overline{\theta}}{\partial x_j}\frac{\partial\overline{\theta}}{\partial x_j}} - \frac{\partial\widehat{\overline{\theta}}}{\partial x_j}\frac{\partial\widehat{\overline{\theta}}}{\partial x_j}$) and the subgrid-scale scalar diffusion ($\nu_T^t\frac{\partial\widehat{\overline{\theta}}}{\partial x_j}\frac{\partial\widehat{\overline{\theta}}}{\partial x_j} - \nu_T^g\widehat{\frac{\partial\overline{\theta}}{\partial x_j}\frac{\partial\overline{\theta}}{\partial x_j}}$) in (2.16) vanish in the laminar flow region. Therefore, in the present method the regions where both the subgrid-scale scalar diffusion and the molecular diffusion vanish, are naturally excluded from the averaging process in (2.16).

	Re_τ	L_x	L_y	L_z	N_x	N_y	N_z	Δx^+	Δy^+	Δz^+
DNS180	180	$2\pi\delta$	2δ	$\pi\delta$	128	128	128	8.8	0.10–7	4.4
LES180F	180	$2\pi\delta$	2δ	$\pi\delta$	48	64	48	23.6	0.60–17	11.7
LES180C	180	$2\pi\delta$	2δ	$\pi\delta$	32	48	32	35.4	0.70–24	17.7
DNS300	300	$2\pi\delta$	2δ	$2\pi/3\delta$	192	192	192	9.8	0.07–5	3.2
LES300	300	$2\pi\delta$	2δ	$2\pi/3\delta$	48	64	48	39.3	0.45–38	13.1

TABLE 1. Grid parameters for large-eddy and direct numerical simulations of turbulent channel flow. L_x, L_y, and L_z are the streamwise, vertical, and spanwise domain sizes, respectively. $N_{x(y,z)}$ and $\Delta x(y,z)^+$ are the number of mesh points and the resolution in wall units, respectively.

3. Results and discussion

Turbulent flow through a plane channel has been widely considered as a benchmark for validating turbulence models. Two different Reynolds numbers of 180 and 300 based on the channel half-height δ and friction velocity u_τ are considered. Two different Pr numbers of 1 and 25 are considered at $Re_\tau = 180$, while only $Pr = 0.72$ is considered at $Re_\tau = 300$. Large-eddy simulation results with the present dynamic model and the dynamic Smagorinsky model (Moin *et al.* 1991) with Lilly (1992)'s modification are compared with direct numerical simulation results. The computational parameters for large-eddy simulations and direct numerical simulations at the two different Reynolds numbers are summarized in table 1. For both the large-eddy and direct numerical simulations, a second-order finite-volume solver (Ham & Iaccarino 2004) on a collocated grid arrangement of the primary variables is employed.

Periodic boundary conditions are imposed in the streamwise and spanwise directions, while no-slip conditions are imposed on the top and bottom walls. The scalar is added to the fluid from the top wall and removed from the bottom wall by using Dirichlet boundary conditions of $\theta_{wall} = \pm 1$. Flow and coordinate variables are normalized by using the friction velocity u_τ $(= \sqrt{\nu(\partial_y \overline{u})_{wall}})$ and the friction scalar θ_τ $(= \alpha(\partial_y \overline{\theta})_{wall}/u_\tau)$.

Figure 1 shows the temporal evolution of the model coefficient for the subgrid-scale scalar flux D_T in turbulent channel flow at $Re_\tau = 180$ after the flow has reached a statistically steady state. The model coefficient for the subgrid-scale scalar flux D_T is found to be dependent on the molecular diffusivity. D_T at $Pr = 1$ ($D_T \sim 1$) is predicted to be smaller than that the value at $Pr = 25$ ($D_T \sim 11$). Furthermore, figure 1 indicates that the model coefficient is dependent on grid resolution.

3.1. *Case A:* $Re_\tau = 180$ *and* $Pr = 1$

In figure 2, the profiles of the mean streamwise velocity, Reynolds shear stress, and rms velocity fluctuations at $Re_\tau = 180$ obtained using the present dynamic model at two different grid resolution (——— and - - - -) and the dynamic Smagorinsky model (·····) are compared with direct numerical simulation data (DNS180, ○). On a coarse mesh (LES180C), the LES results predicted by the present model (- - - -) are comparable to those obtained with the dynamic Smagorinsky model (·····). LES results predicted by the present model are found to converge to the DNS data as the mesh is refined (LES180F).

The present dynamic global-coefficient model predicts the mean scalar and rms scalar

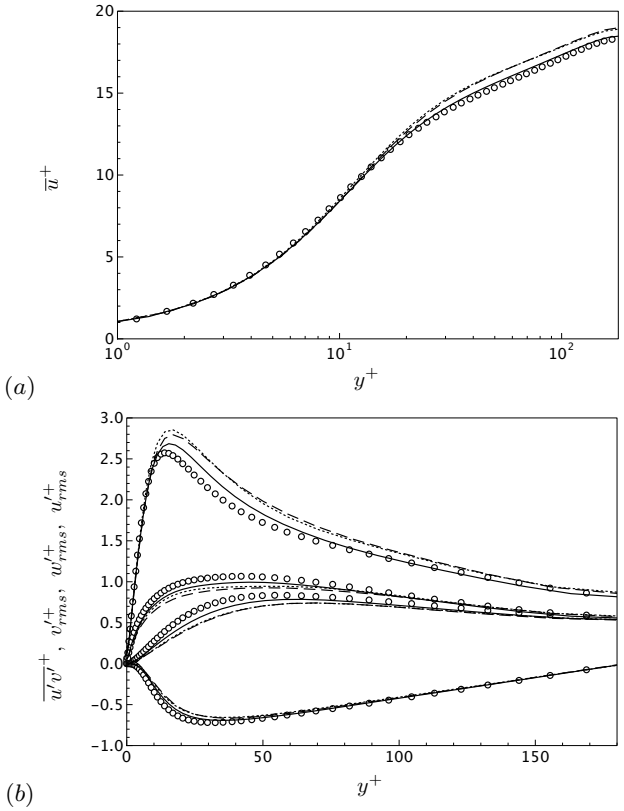

FIGURE 2. Profiles of the (a) mean streamwise velocity and (b) Reynolds shear stress and rms velocity fluctuations in turbulent channel flow at $Re_\tau = 180$ and $Pr = 1$. ——— , the present dynamic model (LES180F); – – – – , the present dynamic model (LES180C); ····· , dynamic Smagorinsky model (LES180C); ∘ , direct numerical simulation (DNS180).

fluctuations with a similar or slightly better accuracy than the dynamic Smagorinsky model predicts, as shown in figure 3. LES results agree well with the DNS data near the wall in the viscous sub-layer, while they deviate from the DNS data away from the wall. LES results predicted by the present model are found to converge to the DNS data with mesh refinement. The present model predicts an overshoot in the peak of $\overline{u'\theta'}^+$ profile, while the overshoot is comparable to that predicted by the dynamic Smagorinsky model. On the other hand, the present model results in favorable prediction of $\overline{v'\theta'}^+$.

Figure 5 shows the profiles of the turbulent Prandtl number, which is defined as:

$$Pr_t = \frac{\overline{u'u'}\frac{d\overline{\theta}}{dy}}{\overline{v'\theta'}\frac{d\overline{u}}{dy}}. \tag{3.1}$$

The present model shows favorable agreement with the DNS in the turbulent Prandtl number, especially near the wall.

3.2. *Case B:* $Re_\tau = 180$ *and* $Pr = 25$

The present dynamic global-coefficient model is also found to predict favorable results at high Prandtl number ($Pr = 25$). It is worth noting that the local equilibrium between

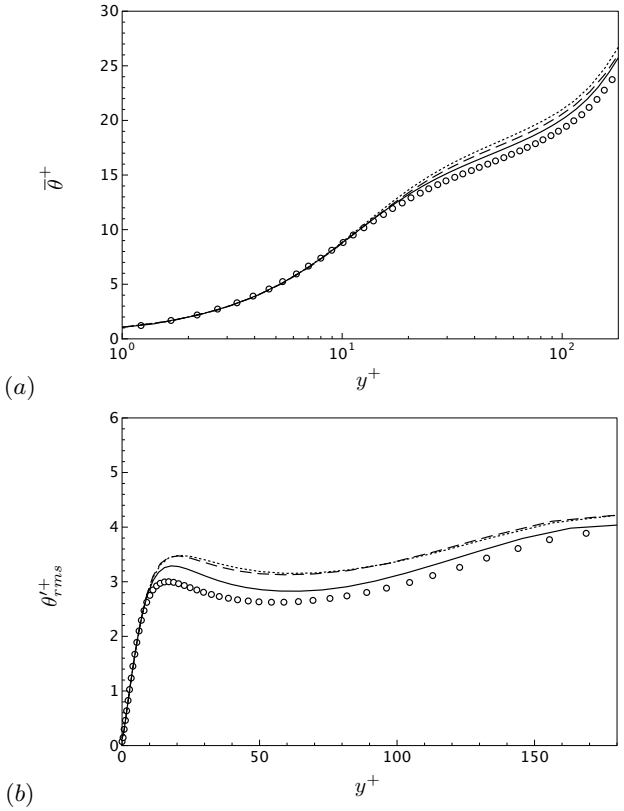

FIGURE 3. Profiles of the (a) mean scalar (b) rms scalar fluctuations in turbulent channel flow at $Re_\tau = 180$ and $Pr = 1$. ——— , the present dynamic model (LES180F); – – – – , the present dynamic model (LES180C); ····· , dynamic Smagorinsky model (LES180C); ∘ , direct numerical simulation (DNS180).

the subgrid-scale scalar diffusion and the molecular diffusion is less likely, especially at high Prandtl (Schmidt) numbers (da Silva & Pereira 2005).

Similarly to the case with $Pr = 1$, the present dynamic gobal-coefficient model predicts the mean scalar and rms scalar fluctuations with a similar to or slightly better accuracy than the dynamic Smagorinsky model predicts, as shown in figure 6. The mean scalar profiles predicted by the present LES agree well with the DNS profile in the viscous sub-layer, while they deviate from the DNS data away from the wall (figure 6(a)). It is found that, in the $Pr = 25$ case, the present model as well as the dynamic Smagorinsky model show better agreement with the DNS result for the rms scalar fluctuations than in the $Pr = 1$ case (figure 6(b)).

Similarly to the case with $Pr = 1$, the present model predicts an overshoot in the peak of $\overline{u'\theta'}^+$ profile (figure 7(a)), while it relatively well predicts $\overline{v'\theta'}^+$ (figure 7(b)). The present model shows favorable agreement with the DNS in the turbulent Prandtl number, especially in the fine mesh simulation (LES180F, ———).

3.3. *Case C:* $Re_\tau = 300$ *and* $Pr = 0.75$

The predictive capability of the present global-coefficient model is also evaluated at a higher Reynolds number ($Re_\tau = 300$). In general, the present model predicts compara-

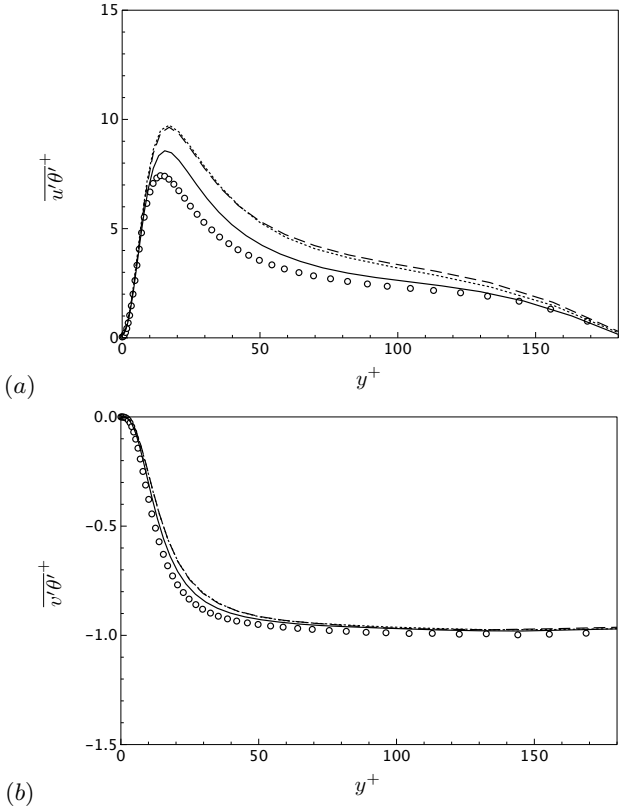

FIGURE 4. Profiles of (*a*) $\overline{u'\theta'}^+$ and (*b*) $\overline{v'\theta'}^+$ in turbulent channel flow at $Re_\tau = 180$ and $Pr = 1$. ——— , the present dynamic model (LES180F); – – – – , the present dynamic model (LES180C); ····· , dynamic Smagorinsky model (LES180C); ∘ , direct numerical simulation (DNS180).

ble results to those predicted by the dynamic Smagorinsky model in terms of the mean and turbulent velocity and scalar quantities. The present model as well as the dynamic Smagorinsky model are found to predict overshoots in the log-layers of the mean velocity (figure 9(*a*)) and scalar profiles (figure 10(*a*)). The present model shows consistent predictive behavior observed in the simulations at lower Reynolds number ($Re_\tau = 180$) in the prediction of the rms velocity (figure 9(*b*)) and scalar fluctuations (figure 10(*b*)).

Similarly to the case with $Re_\tau = 180$, the present model predicts an overshoot in the peak of $\overline{u'\theta'}^+$ profile (figure 11(*a*)), while it relatively well predicts $\overline{v'\theta'}^+$ (figure 11(*b*)).

4. Conclusions

The dynamic global-coefficient subgrid-scale eddy-viscosity model by You & Moin [Phys. Fluids **19**, 065110 (2007)] has been generalized for large-eddy simulation of turbulent flow with scalar transport. The model coefficients for eddy viscosity and subgrid-scale scalar flux which are globally constant in space but vary in time are dynamically determined based on the "global conservation" of transport equations for the trace of Germano identity and scalar variance, respectively. Large-eddy simulations of turbulent channel flow show that the present model has a similar predictive capability to the dynamic Smagorinsky model of Moin *et al.* [Phys. Fluids A **3**, pp. 2746 (1991)] for both

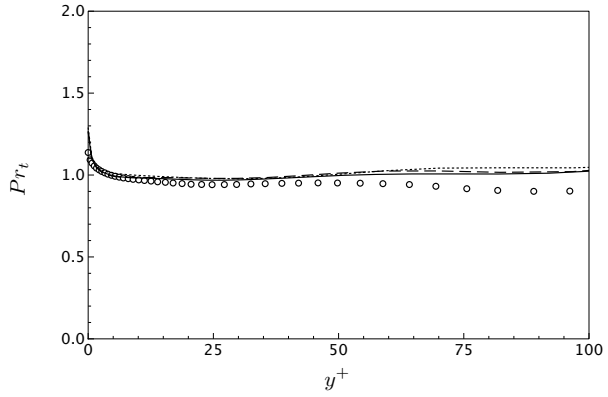

FIGURE 5. Profiles of turbulent Prandtl number in turbulent channel flow at $Re_\tau = 180$ and $Pr = 1$. ——— , the present dynamic model (LES180F); – – – – , the present dynamic model (LES180C); ····· , dynamic Smagorinsky model (LES180C); ∘ , direct numerical simulation (DNS180).

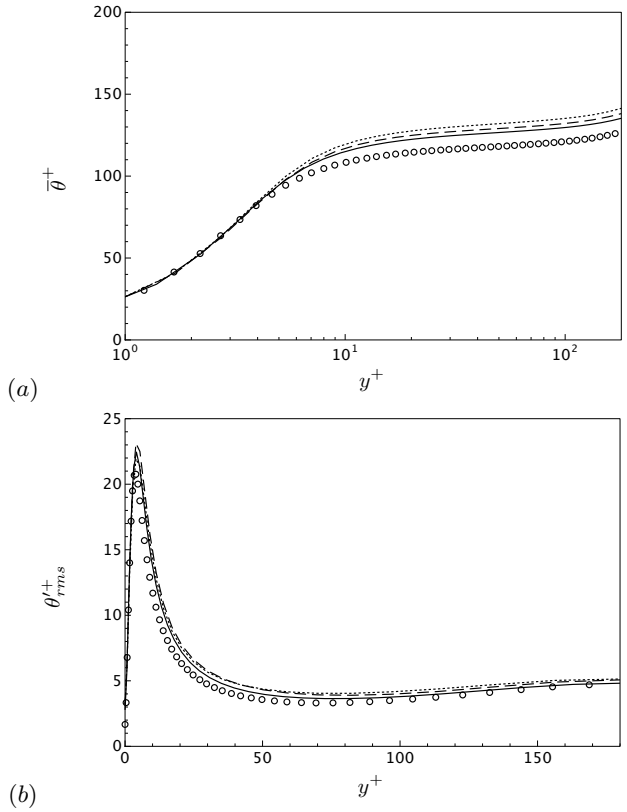

FIGURE 6. Profiles of the (a) mean scalar (b) rms scalar fluctuations in turbulent channel flow at $Re_\tau = 180$ and $Pr = 25$. ——— , the present dynamic model (LES180F); – – – – , the present dynamic model (LES180C); ····· , dynamic Smagorinsky model (LES180C); ∘ , direct numerical simulation (DNS180).

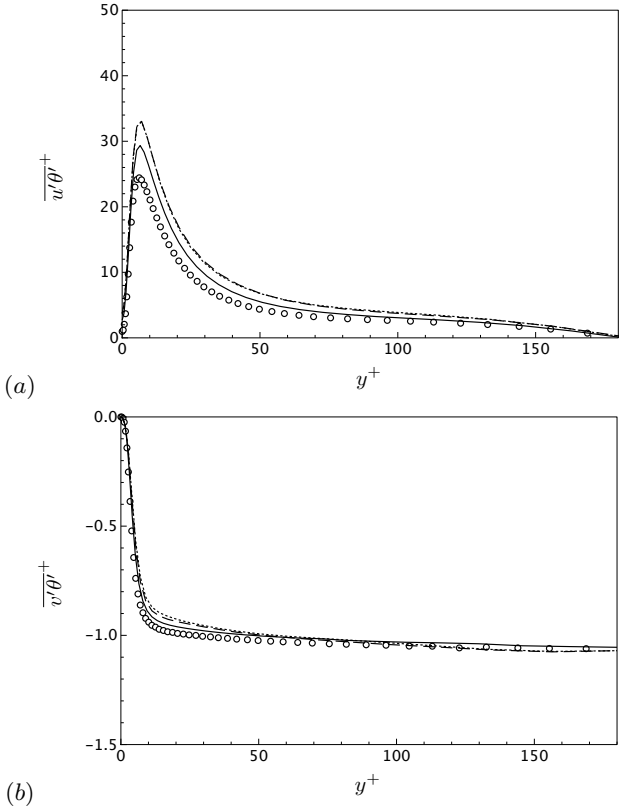

FIGURE 7. Profiles of (*a*) $\overline{u'\theta'}^+$ and (*b*) $\overline{v'\theta'}^+$ in turbulent channel flow at $Re_\tau = 180$ and $Pr = 25$. ——— , the present dynamic model (LES180F); – – – – , the present dynamic model (LES180C); ····· , dynamic Smagorinsky model (LES180C); ∘ , direct numerical simulation (DNS180).

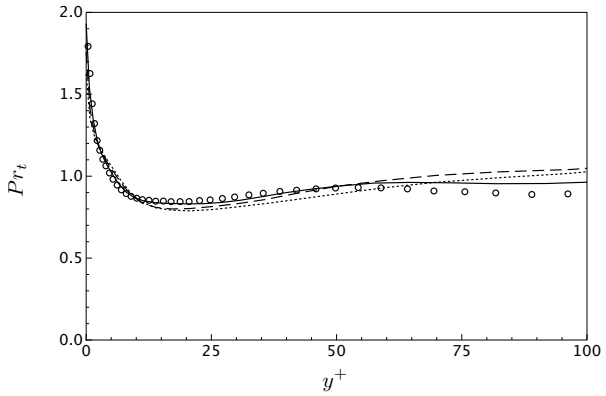

FIGURE 8. Profiles of turbulent Prandtl number in turbulent channel flow at $Re_\tau = 180$ and $Pr = 25$. ——— , the present dynamic model (LES180F); – – – – , the present dynamic model (LES180C); ····· , dynamic Smagorinsky model (LES180C); ∘ , direct numerical simulation (DNS180).

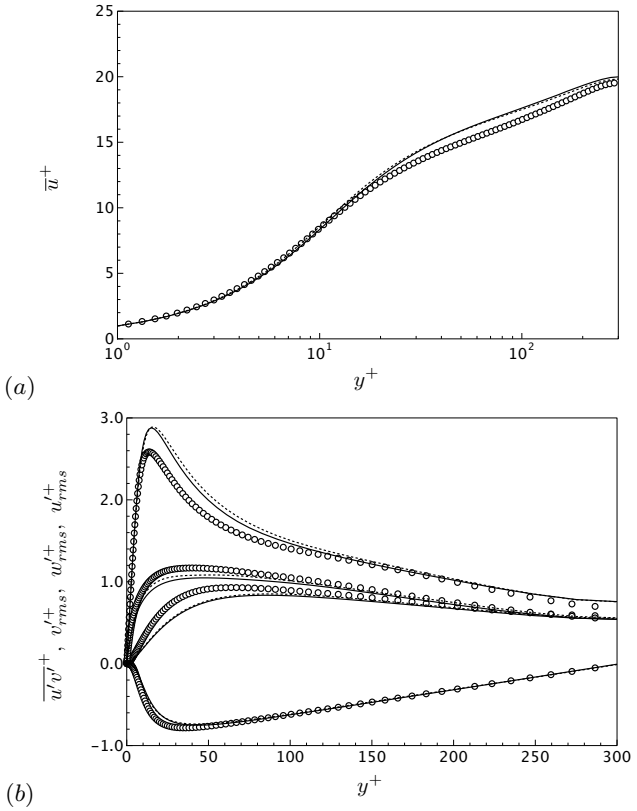

FIGURE 9. Profiles of the (a) mean streamwise velocity and (b) Reynolds shear stress and rms velocity fluctuations in turbulent channel flow at $Re_\tau = 300$ and $Pr = 0.72$. ——— , the present dynamic model (LES300); ····· , dynamic Smagorinsky model (LES300); ∘ , direct numerical simulation (DNS300).

turbulent velocity and scalar fields. The present dynamic model is especially suitable for large-eddy simulation of turbulent flow with scalar transport in complex geometries since it does not require any *ad hoc* spatial and temporal averaging or clipping of the model coefficient for numerical stabilization, and requires only a single-level test filter. The present model is not more complicated in implementation and not more expensive in terms of the computational cost than the dynamic Smagorinsky model.

Acknowledgments

The authors gratefully acknowledge the support from the Boeing Company and the Advanced Simulation and Computing Program of the U. S. Department of Energy.

REFERENCES

BORUE, V. & ORSZAG, S. A. 1998 Local energy flux and subgrid-scale statistics in three-dimensional turbulence. *Journal of Fluid Mechanics* **366**, 1–31.

DA SILVA, C. B. & METAIS, O. 2002 On the influence of coherent structures upon

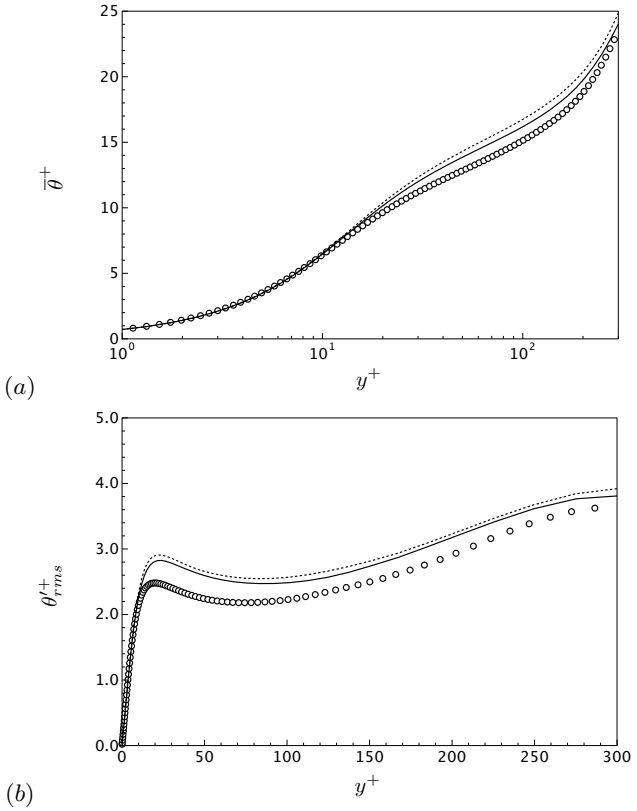

FIGURE 10. Profiles of the (a) mean scalar (b) rms scalar fluctuations in turbulent channel flow at $Re_\tau = 300$ and $Pr = 0.72$. ——— , the present dynamic model (LES300); ····· , dynamic Smagorinsky model (LES300); ∘ , direct numerical simulation (DNS300).

interscale interaction in turbulent plane jets. *Journal of Fluid Mechanics* **473**, 103–145.

DA SILVA, C. B. & PEREIRA, J. C. F. 2005 On the local equilibrium of the subgrid scales: The velocity and scalar fields. *Physics of Fluids* **17**, 108103.

GERMANO, M., PIOMELLI, U., MOIN, P. & CABOT, W. H. 1991 A dynamic subgrid-scale eddy-viscosity model. *Physics of Fluids (A)* **3** (7), 1760–1765.

HAM, F. & IACCARINO, G. 2004 Energy conservation in collocated discretization schemes on unstructured meshes. Annual Research Briefs, 3-14. Center for Turbulence Research, Stanford, California.

LILLY, D. K. 1992 A proposed modification of the Germano subgrid-scale closure model. *Physics of Fluids (A)* **4** (3), 633–635.

MENEVEAU, C., LUND, T. S. & CABOT, W. H. 1996 A Lagrangian dynamic subgrid-scale model of turbulence. *Journal of Fluid Mechanics* **319**, 353–385.

MOIN, P., SQUIRES, K., CABOT, W. & LEE, S. 1991 A dynamic subgrid-scale model for compressible turbulence and scalar transport. *Physics of Fluids (A)* **3**, 2746.

MOSER, R. D., KIM, J. & MANSOUR, N. N. 1999 Direct numerical simulation of turbulent channel flow up to Re_τ=590. *Physics of Fluids* **11** (4), 943–945.

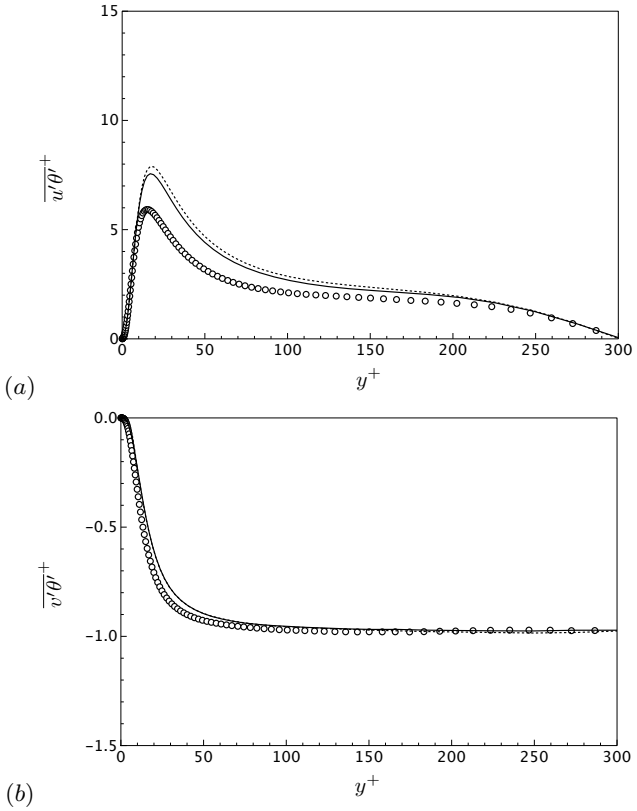

FIGURE 11. Profiles of (*a*) $\overline{u'\theta'}^+$ and (*b*) $\overline{v'\theta'}^+$ in turbulent channel flow at $Re_\tau = 300$ and $Pr = 0.72$. ——— , the present dynamic model (LES300); ····· , dynamic Smagorinsky model (LES300); ∘ , direct numerical simulation (DNS300).

PARK, N., LEE, S., LEE, J. & CHOI, H. 2006 A dynamic subgrid-scale eddy-viscosity model with a global model coefficient. *Physics of Fluids* **18**, 125109.

VREMAN, A. W. 2004 An eddy-viscosity subgrid-scale model for turbulent shear flow: algebraic theory and applications. *Physics of Fluids* **16** (10), 3670–3681.

YOU, D. & MOIN, P. 2007 A dynamic global-coefficient subgrid-scale eddy-viscosity model for large-eddy simulation in complex geometries. *Physics of Fluids* **19** (6), 065110.